NUMERICAL SIMULATION OF RADIATIVE HEAT TRANSFER IN A BINARY-SIZE GRANULAR BED

by

Tianhua ZHANG[a,c], Chuanping LIU[b*], Huigang WANG[c*], Min GUO[a], and Mei ZHANG[a]

[a]State Key Laboratory of Advanced Metallurgy, School of Metallurgical and Ecological Engineering, University of Science and Technology Beijing, Haidian District, Beijing, China
[b]School of Energy and Environmental Engineering, University of Science and Technology Beijing, Haidian District, Beijing, China
[c]Central Research Institute of Building and Construction Co., Ltd., MCC Group, Haidian District, Beijing, China

Original scientific paper
https://doi.org/10.2298/TSCI220204091Z

The radiative heat transfer in a high temperature granular bed of binary-size mixture was explored in this paper. The effective view factor between particles decreases exponentially with the increase in particle interval, increases with the increase in the size of the absorption particle but is hardly affected by the volume ratio of the mixture. The effective thermal conductivity of granular bed was further deduced basing on the characteristic of the effective view factor. It is indicated that the thermal conductivity is proportional to the particle size and temperature cubed, and increases with the increase in the particle size ratio and volume ratio. Finally, modified calculation correlations of the effective view factor and effective thermal conductivity were developed for binary-size bed based on the simulation results, and good accuracy of less than 0.01 and 10% had been achieved, respectively.

Key words: *effective view factor, effective thermal conductivity, granular bed, binary-size mixture*

Introduction

Granular bed is widely used as heat storage and heat transfer device in the fields of the chemical industry, energy, metallurgy, and so on because of its simple structure, convenient operation, and high thermal efficiency. Heat exchange happens between particles, which normally consists of three parts [1], as the conduction through physical contact of particles, the conduction through the fluid gap among particles, and the thermal radiation between particles. Thermal radiation is an important part of heat transfer in high temperature granular systems, such as the packed pebble bed of high temperature gas-cooled reactor [2], blast furnace [3], bubbling fluidized bed [4], and other packed granular beds. It exists between the contacting or adjacent particles as well as the non-contacting particles [5-7], which can be ignored when the bed temperature is low, however, it becomes the dominant mode when the temperature increases over 800 °C.

*Corresponding authors, e-mail: cpliu@ustb.edu.cn, wanghuigang0822@126.com

Effective thermal conductivity of radiation, k_r, is an important parameter for the thermal design of high temperature beds, which was received extensive attention [8, 9]. Chen *et al.* [10] obtained the view factor by regarding the radiative heat transfer of particle material as a diffuse reflection process, and the results showed the factor is related to the absorptivity and scattering rate of particle material. Argo and Smith [11], Wakao and Kato [12], Kasparek *et al.* [13], Vortmeyer *et al.* [14], and others also gave empirical calculation formulas of view factor, which could be suitable for a specific bed void fraction. Antwerpen *et al.* [15] used a multi-sphere element model to study the effective thermal conductivity of a single-size granular bed. Johnson *et al.* [16] discussed the effect of bed void fraction and material emissivity on the effective thermal conductivity of radiation. Zhou *et al.* [17] proposed a 2-D boundary element method to calculate the effective thermal conductivity of a granular bed. The results showed that radiation made a very important influence on the effective thermal conductivity under high temperatures, and both the particle size and particle thermal conductivity affected the thermal conductivity of the bed. Singh *et al.* [18] studied the effect of the particle material on the effective thermal conductivity of radiation. During the radiation process in the bed, the particles absorb rays and then radiate outward again from the other side, which is affected by the conductivity of particle material to a certain extent.

The aforementioned studies mostly focused on the thermal conductivity of radiation in a single-size granular bed. In the actual process, the particles used in the bed usually have a certain size distribution. In the multi size granular bed, the particles of different diameter shield each other, which change the heat transfer of radiation, thereby affecting the effective thermal conductivity of radiation of the bed. It is necessary to clarify the effect of the size composition of particles on the radiative heat transfer of the bed. Chen *et al.* [19, 20] studied the particle contact conduction of binary granular bed at the temperature range of 500~530 °C, and found that the bed had the largest effective thermal conductivity when the solid fraction of large particles is 60%. Mandal *et al.* [21] discussed the relationship between void fraction and effective thermal conductivity in a 30 °C bed, and pointed out that the effective thermal conductivity reached the maximum when the void fraction was the smallest. However, there is little research about thermal radiation in the high temperature granular mixture.

This paper conducts research on the granular bed of binary-size particles with high temperature, introduces the Monte-Carlo (MC) method [22-24] to estimate the radiative heat transfer between particles, analyzes and obtains the calculation formula of effective thermal conductivity, and provides a calculation basis for the radiative heat transfer of binary- and multi-size granular bed.

Model establishment and calculation

There where several models of multiple-body radiation within the packed granular bed, *i.e.*, black radiation model, uniform radiation model, local radiation model, particle scale radiation model (PSRM), and so on [9]. The black model is only valid for an emissivity of 1. The uniform radiation model is also not appropriate for modeling gray particles because of the assumption of uniform radiosity on the particle surface. The local radiation model, where each particle surface is divided into many surface elements, improves upon the uniform radiation model, but the high computational cost of calculating radiation element-by-element makes this unsuitable for a granular bed with lots of particles. According to Wu's [9] suggestion, the PSRM had a good approximation of the local radiation model. Hence, the PSRM was adopted to simulate the radiative heat transfer in this paper.

The framework of the simulation in this paper was shown in fig. 1:

- A computation domain randomly packed with particles is generated by using discrete element method (DEM).
- A MC method is used to solve the *effective view factor* between particles.
- Based on the PSRM, a radiative heat transfer simulation is run in domain where the left side is heated and the right is cooled.
- The resulting steady-state temperature profile is plotted and fitted by a curve of fourth power of particle temperature, T^4, and then the effective thermal conductivity k_r can be calculated.

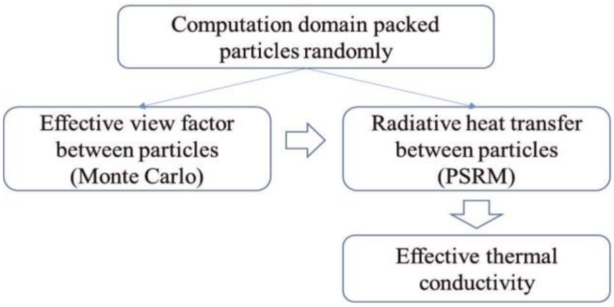

Figure 1. Framework of simulation

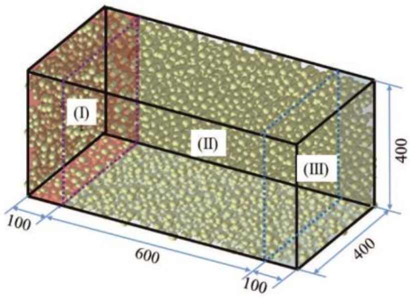

Figure 2. Computation domain of radiation

Computation domain

A packed bed was generated by the DEM, where the particles were distributed randomly and packed loosely and the solid fraction, φ, was about 0.52. The particles collided each other and the Hertz force model with a Young's modules of 10^9 and restitution coefficient of 0.5 was adopted to simulate the particle collision. A rectangle of 800 mm width, 400 mm height, and 400 mm thickness was cut from the packed bed as computation domain, as shown in fig. 2. Uniform cubic cells of 1.25 diameter of small particle (1.25 d_1) were meshed to track the particle position. The domain had periodic boundaries in the height and thickness directions. The particles at the boundaries contacted with that at the opposite and the particles leaving out the boundaries would re-enter at the opposite direction.

To deduce the effective thermal conductivity, the domain was divided into three parts from left side to right, fig.2:
- radiation-emitting region of 100 mm width (Region I),
- radiation-transmitting region of 600 mm width (Region II), and
- radiation-absorbing region of 100 mm width (Region III).

The heat is transferred from the region I to III.

Effective view factor

The particle (emitter) in bed emitted rays from its surface. The ray followed its path and reached the surface of the neighbors. Part of the ray was absorbed, and the unabsorbed part formed a diffuse reflection. Here, the assumption of no transmission through particles and a non-participating fluid phase was considered, and the emissivity and absorptivity met the Kirchhoff's law. The effective view factor, F, was defined as the ratio of the energy absorbed by a particle from the emitter and the total emitting energy, depicting the influence of the particle interval on radiation in granular bed.

Several methods were developed to solve the radiative heat transfer in the literatures, as the discrete ordinates method (DOM) [25], finite volume method (FVM) [26], and MC integration [27]. In DOM and FVM, the domain was divided into a finite number of control volumes, resulting in the flase scattering and ray effect (consequence of spatial discretization and angular discretization, respectively). Because of the simple algorithm and flexibility to real physical conditions, MC technique was broadly served as a reference to other methods [28]. Here, the solution of MC was used to find the effective view factor between particles in binary size granular bed.

The basic calculation process of the MC method was, as shown in fig. 3(a):

– Determining a particle p_o in the center of the computation domain as the emitter.
– Selecting a radiation point randomly on the surface of the emitter, and emitting a ray randomly from the point to the hemispherical space.
– Tracking the possible path of the ray and finding the second particle and the landing point that the ray reaches.
– Part of the ray is absorbed according to the absorptivity and the remaining part is diffusely reflected.
– Emitting a diffuse reflection ray from landing point.
– Continuing to track the diffuse reflection ray, and finding the particles, which are absorbed the reflection ray. The energy of the diffuse reflection ray is relatively lower; therefore, the re-reflection can be ignored, *i.e.*, all the diffuse reflection ray is absorbed by the particle surface.
– Summating the radiative rays and reflection rays absorbed particle by particle after the rays are enough in statistics.

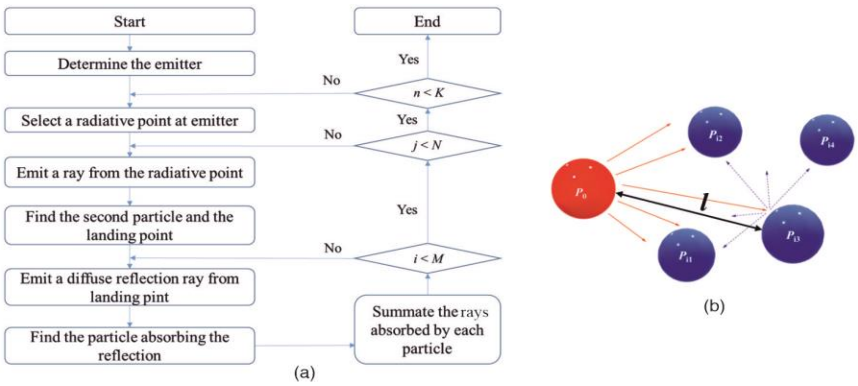

Figure 3. Calculation of view factor; (a) schematic map of MC and (b) the radiation transmission (red line), and diffuse reflection transmission (blue line)
(*for color image see journal web site*)

The C++ was used to MC code. Once the number of radiative points, radiative rays and reflection rays were sufficient (K, N, and M in fig. 3, respectively), a statistically calculation result could be obtained, and the output of the MC code was the radiation distribution factor (RDF), the proportion of the rays from the emitter and that absorbed by the particles after a number of reflections, which was termed as effective view factor. The effective view factor, F, was given:

$$F = \frac{k_1 \alpha_{r,i} + k_2 (1 - \alpha_{r,i}) / M}{k_0} \tag{1}$$

where $\alpha_{r,i}$ was the absorptivity of particle i (p_{i}), k_0 – the number of radiative rays emitted by emitter p_{o}, k_1 and k_2 – the absorption rays and reflection rays by particle i, respectively, and M – the reflection number for each ray.

The interval between the particle p_{o} (emitter) and the particle p_{i} (absorber) is marked as l, fig. 3(b). As l increases, the radiation rays absorbed by p_{i} decreases, and F decreases accordingly.

Radiative heat transfer between particles

The computation domain was divided into three parts, as shown in fig. 2. The particles in Regions I and Region III had a fixed temperature T_h and T_l, respectively. As $T_h > T_l$, the heat transferred from Region I-III. No heat conduction and heat convection occurred between the particles, and here only radiative heat transfer was considered. The radiative heat exchange between particle i and particle j ($q_{r,ij}$) was calculated according to [6]:

$$q_{r,ij} = \frac{\sigma(T_j^4 - T_i^4)}{\dfrac{1-\alpha_{r,i}}{\alpha_{r,i} A_i} + \dfrac{1}{A_i F_{i,j}} + \dfrac{1-\alpha_{r,j}}{\alpha_{r,j} A_i}} \tag{2}$$

where T [K] was the particle temperature, σ [m^{2}K^4] (= 5.67×10^{-8}) – the Stefan-Bolzmann constant, A [m^2] (= 0.5πd^2) – the radiation area of the particle, d [m] – the particle diameter, subscripts i and j represent particles i and j, respectively, and $F_{i,j}$ – the effective view factor between particles i and j.

According to the energy balance, the temperature of the particle i in Region II was changed (3):

$$m_i C_{p,p,i} \frac{\mathrm{d}T_i}{\mathrm{d}t} = \sum_{j=1}^{n} q_{r,ij} \tag{3}$$

where m_i [kg], $C_{p,p,I}$ [Jkg^{-1}K^{-1}], and T_i [K] were the mass, specific heat, and temperature of particle i, respectively, n – the number of particles contacting with particle I, and $q_{r,ij}$ [W] – the heat exchange between particle i and particles j.

The T_i was adjusted after every time step t_{step}:

$$T_{i,\mathrm{final}} = T_{i,\mathrm{initial}} + t_{\mathrm{step}} \frac{\mathrm{d}T_i}{\mathrm{d}t} \tag{4}$$

where $T_{i,\mathrm{final}}$ [K] and $T_{i,\mathrm{initial}}$ [K] were the temperature of particle i at final and initial time.

The total radiative heat flux Q [W] between Regions I and II, $Q_{\mathrm{I,II}}$, (or Regions II and III, $Q_{\mathrm{II,III}}$) could be summarized particle by particle:

$$Q_{\mathrm{I,II}} = \sum_{i\in\mathrm{I}} \sum_{j\in\mathrm{II}} q_{r,ij}, \quad Q_{\mathrm{II,III}} = \sum_{i\in\mathrm{II}} \sum_{j\in\mathrm{III}} q_{r,ij} \tag{5}$$

Effective thermal conductivity

After stabilization, $Q_{\mathrm{I,II}} = Q_{\mathrm{II,III}}$ and the temperature distribution in the Region II was obtained, as $T = f(x)$, where x was the position of particles in width direction. The effective thermal conductivity of radiation $k_{r,\mathrm{eff}}$ could be obtained based on the following expression:

$$k_{r,\mathrm{eff}} = \frac{Q}{A_D \partial T / \partial x} \tag{6}$$

where A_D (= 0.16 m^2) was the cross-sectional area of the computation domain, $\partial T/\partial x$ [Km^{-1}] – the temperature gradient of particles in the Region II, K·m^{-1}, Q [W] – the heat flux between regions, $Q = Q_{\mathrm{I,II}} = Q_{\mathrm{II,III}}$ after stabilization.

Results and discussion

Effective view factor calculation

The effective view factor of the single-size granular bed was firstly calculated based on the theory in section *Effective view facto*r before calculating the view factor of the binary-size bed, verifying its feasibility.

Single size granular bed

Single-size particles of 40 mm diameter were randomly packed in the domain. The relationship between the view factor and the dimensionless particle interval (ratio of particle interval to particle diameter, $L = l/d$) is shown in fig. 4(a). The results indicate that the view factor has the largest value when the absorber are in contact with emitter ($L = 0$). The effective view factor decreases exponentially with the increase in L, and it is almost completely attenuated ($F \approx 0$) when L is greater than 1. The calculation can be repeatedly conducted, which shows that the random packing of particles does not affect the relationship of F~L.

Figure 4(b) shows the relationship of F~L at different absorptivities, where all the value are the average view factor at the same position. It can be seen that the view factor also decreases exponentially with the increase in particle interval no matter how the absorptivity varies. In addition, Figure 4(b) also indicates that the effective view factor decreases with the decrease in absorptivity.

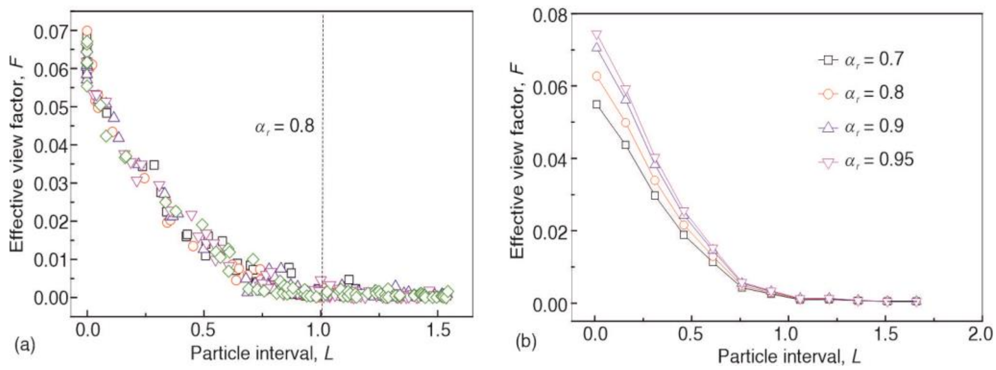

Figure 4. Effective view factor of the particles in the granular bed, $L = l/d$; (*a*) □, ○, △, ▽, and ◇ represent five different accumulation of particles and (*b*) the relationship between view factor and particle interval under different α_r

Validation of MC model

To validate the MC model used in this paper, the calculation results of the relationship of F~L were compared to that calculated by Pitso [5] and Johnson *et al*. [16], as shown in fig. 5. The comparisons were illustrated that the effective view factor had almost the same changing trend as that reported in [5, 16]. Therefore, the calculation method proposed in this paper was feasibility. Then, the effective view factor of binary-size granular bed was further calculated on the basis of that of the single-size bed.

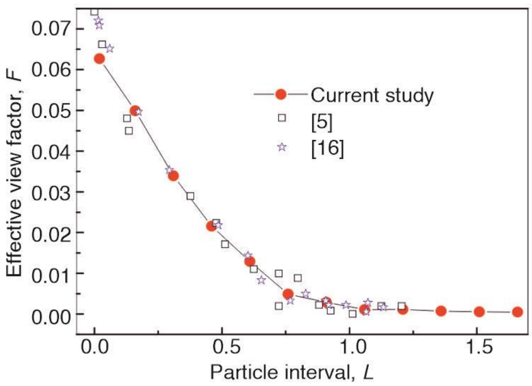

Figure 5. Comparison of the effective view factor calculating in this work with others, α_r = 0.8

Binary size particle bed

The small particles (d_1 = 20 mm) were mixed with the large ones (d_2 = 40, 30, and 26.6 mm, respectively) in the same proportion of volume ($V_2 = V_1$, V_2, and V_1 are the total volume of large and small particles in the bed, respectively) and then randomly packed in the calculation bed. The radiation rays emitted from the emitter, p_o, and then were absorbed by the rest of the particles in the computation domain.

Figure 6 presents the view factor of the absorber in different binary mixtures, where D is the size ratio of large and small particles, $D = d_2/d_1$. The results show that the absorption energy decreases exponentially with the increase in L whether the absorber is a large particle or a small. The large particle has a larger surface than the small; therefore, the large particle absorbs more radiation energy under the same conditions. That is to say, the absorption radiation energy by large particles is greater than that by small ones at the same interval, resulting in that the effective view factor is larger, fig. 6. For an example, the effective view factor of large particles is 0.015 larger than that of small particles when D = 1.33 and L = 0, fig. 6(c). With the increase in D, the gap of the effective view factor becomes large moderately. Specifically, the effective view factor gap is 0.024 when D = 1.5, fig. 6(b), and 0.045 when D = 2, fig. 6(a). The increasing ratio of the effective view factor (F_l/F_s, F_l, and F_s are the view factor of large and small particles) is smaller than the size ratio of particles D, which may be ascribed to the shielding between particles.

Figure 7 shows the relationship of F~L at different fraction ratios of large and small particles ($\Omega = V_2/V_1$). Under the same calculated conditions, the large particles always absorbed more radiation energy than the small ones, that was, the effective view factor of large particles was larger than that of small ones. But for each particle, the relationship of F~L was hardly affected by Ω whether the absorber is a large or a small particle. In this calculation of D = 2, the relationship of F~L hardly changed when the solid fraction ratio Ω increased from 1 to 3. In other words, for the binary-size granular bed, the effective view factor was only affected by the particle size ratio D, not the solid fraction ratio Ω.

Correction of effective view factor

According to the results in sections Single size granular bed and *Binary size particle bed*, the absorber contacted with emitter receive the most rays and has the largest effective view factor. With interval L increasing, the effective view factor decreases rapidly and tend to 0. The RDF seemly conforms to a normal distribution, hence the relationship of F~L is assumed as the following relationship:

$$F = \frac{1}{n_2\sqrt{2\pi}\theta}\exp\left(-\frac{L^2}{2\theta^2}\right) \tag{7}$$

where n_2 is the number density of absorber at l, $n_2 = 6\varphi(2L + D + 1)^2/D^3$; φ = 0.52, $L = l/d$, $D = d_2/d_1$, and θ is the standard deviation of the distribution.

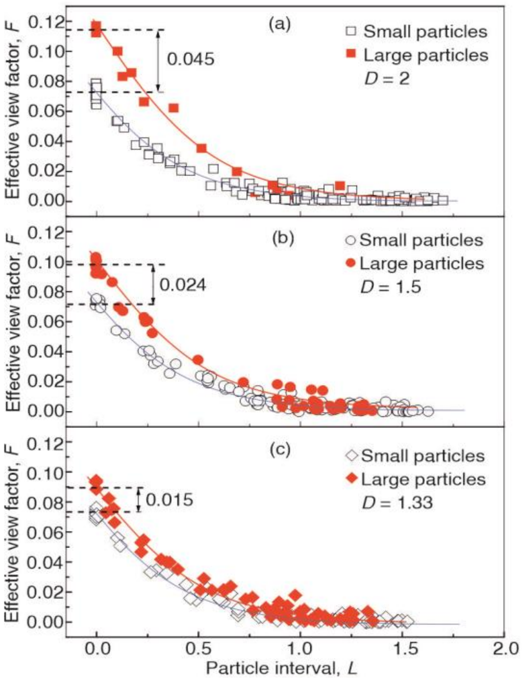

Figure 6. Relationship between effective view factor and particle interval under different diameter ratio, $V_2 = V_1$, $\alpha_r = 0.9$, $d_1 = 20$ mm

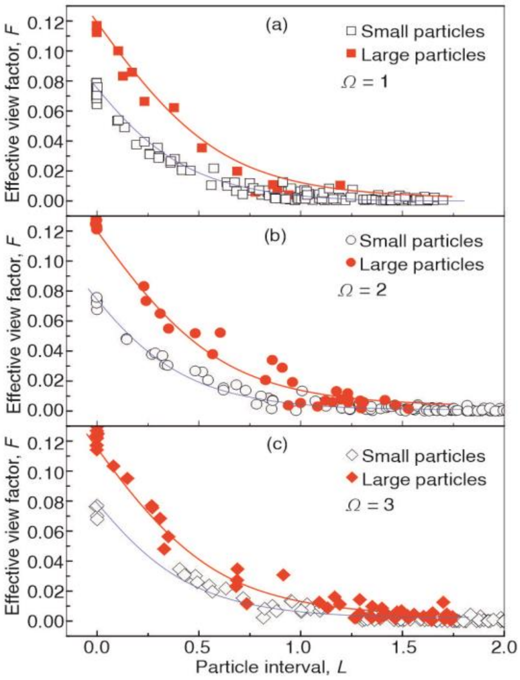

Figure 7. Relationship between effective view factor and particle interval under different solid fraction ratio, $D = 2$, $\alpha_r = 0.9$, $d_1 = 20$ mm

The F is influenced by particle interval L, absorptivity α_r, and particle size ratio D. The relationship of eq. (7) presents the effect of L. Then it is considered that θ is related to α_r and D, and shows the simple function as:

$$\theta = a(\alpha_r)^b D^c \tag{8}$$

where a is the proportional coefficient, b and c are the exponential coefficients.

The simulation results of effective view factor for binary size granular bed are presented in section *Single size granular bed* and *Binary size particle bed*. Based on these MC simulation results, a, b, and c can be got by fitting eqs. (7) and (8), and their value is 0.388, –0.962 and 1.333, respectively.

Figure 8 gives the fitting accuracy of eq. (7). Most of the fitting results are in good agreement with the original value from the MC simulation, where the fitting error of effective view factor is within 0.01. As the original view factor has a certain of deviation, the data in figs. 4, 6, and 7, and the effects of α_r, D, and Ω on view factor are complex, a small number of data are out of the range of ±0.01. As there are several thousand particles in computation domain, the error will be weakened. Here, eq. (7) is subsequently used to estimate the effective radiation thermal conductivity of granular bed in the next section.

Temperature distribution and effective thermal conductivity

Radiative heat transfer and PSRM

Small particles of d_1 were mixed with large ones of d_2 in a volume proportion Ω and then randomly packed in a granular bed. At the initial moment (t = 0 seconds), the temperature of the particles in Zone I was initiated as 1000 K, and those in Zones II and III were both 800 K, fig. 9(a). During the process of heat transfer, the temperature of the particles in Zones I and III remained unchanged. The temperature in Zone II began to increase with the proceeding of the radiative heat transfer between particles. The temperature distribution in the bed at different times was shown in fig. 9(a). The temperature of the particles in Zone II gradually increased from right to left, and showed sunken distribution. In addition, it also could be seen that the temperature distribution in the bed after 10000 seconds was almost similar to that of 15000 seconds. Therefore, it could be considered that the temperature distribution became stable after 10000 seconds, and the temperature cloud diagram was shown in the insert of fig. 9(a) after stabilization. Wigh the periodic boundary, the temperature gradient only exists in the width direction (x-direction) and no gradient in the height and thickness directions.

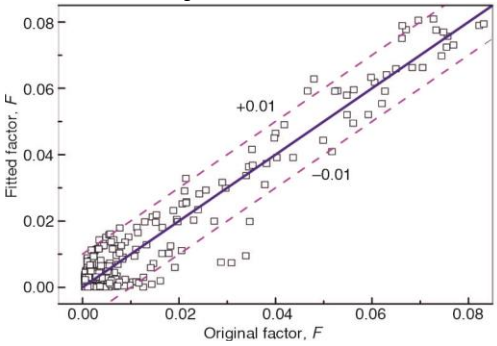

Figure 8. The fitting results of eq. (7) and the original results from the MC method

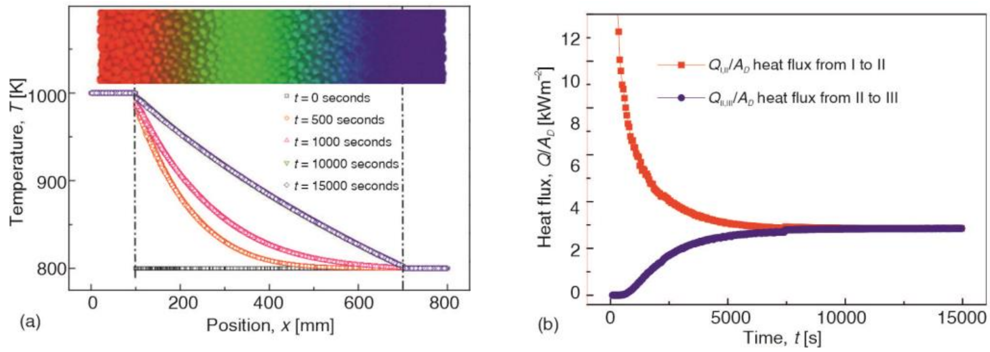

Figrку 9. Heat transfer calculation of granular bed, α_r = 0.95; (*a*) change of temperature distribution and (*b*) relationship between heat flux and time: d_1 = 20 mm, d_2 = 40 mm, Ω = 1, α_r = 0.95

The radiation heat fluxes between Zones I and II, II and III are shown in fig. 9(b). The calculation results indicated that the heat flux between I and II, $q_{\mathrm{I,II}}$, gradually decreased, while the heat flux between II and III, $q_{\mathrm{II,III}}$, increased as the heat transfer went on. Finally, $q_{\mathrm{I,II}}$ and $q_{\mathrm{II,III}}$ reached uniformity after stabilization.

The temperature distribution (relationship between the particle temperature and its position) in Zone II after stabilization is given as $f(T, x) = 0$. According to the fitting data, the fourth power of particle temperature, T^4, shows a linear relationship with its position along x-direction, as $T^4 = ax+b$.

Based on the eq. (6), the effective thermal conductivity can be further given as:

$$k_{r,\mathrm{eff}} = \frac{4}{a}\frac{Q}{A_D}T^3 \tag{9}$$

where a and b are parameters according to data fitting. Equation (9) shows that the effective thermal conductivity is proportional to T^3, which is consistent with the literatures [13, 14].

Figure 10 presents the temperature distribution and the corresponding effective thermal conductivity for the granular mixture of 20 mm and 40 mm. As the bed temperature increases from 800 K to 1000 K, the effective thermal conductivity increases from 11.4-22.0 W/mK, while the temperature gradient in the Region II decreases.

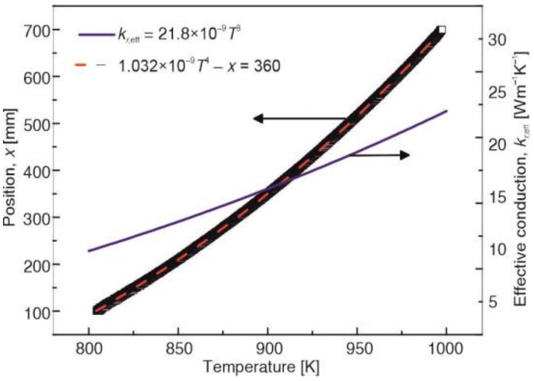

Figure 10. Effective radiation thermal conductivity of bed; α_r = 0.95, d_1 = 20 mm, d_2 = 40 mm, Ω = 1

Effective thermal conductivity

Figure 11 shows the temperature distribution of granular mixture after stabilization under different calculation conditions. The results indicated that the temperature distribution of particles in bed is hardly affected by particle diameter, d, particle size ratio, D, volume ratio, Ω, and absorptivity, α_r. The temperature distribution in fig. 11 is completely coincident with that in fig. 10. So it can be considered that T^4 is always in liner with the position in the x-direction, and the thermal conductivity is a third power relationship of temperature.

Figure 12(a) gives the effective thermal conductivity in a single-size granular bed, indicating that the effective thermal conductivity increases linearly with the particle size. Although the temperature distribution is almost unaffected by the particle size, the large size particle will bring in a large temperature difference between adjacent particles and a great heat transfer Q, resulting the large $k_{r,\mathrm{eff}}$. The effective thermal conductivity in a binary size granular bed is given in fig. 12(b)-12(d). The results indicated that the absorptivity of particles has a small effect on thermal conductivity. When the absorptivity increases, the radiation reflection decreases, and the effective thermal conductivity decreases slightly. The heat flux transferred by the large particles increases when the size of large particles increases or the volume ratio of large particles increases, resulting in the increase of thermal conductivity in the bed.

Validation of numerical model

There are some empirical formulas to calculate the thermal conductivity of the packed bed of single size particles, as the model of Zehner, Bauer, and Schlunder (ZBS) [29], Breitbach and Bartheles (BB) [30], Wakao and Kato (WK) [12], and so on. Here, we comparing our simulation results with the previous, as shown in fig. 13. Comparatively speaking, the thermal conductivity of WK is much lower than the others, as the effect of solid fraction φ does not considered. For the loose packed bed with φ = 0.52, $k_{r,\mathrm{eff}}$ in the current study is closed to that calculated by ZBS and BB, and the difference is less than 10% during the temperature range from 800-1000 K. The difference may be induced by the fitting error of eq. (4), and it can be considered that the numerical model in this study predicts the effective heat conductivity of radiation well.

Correction of effective thermal conductivity

In our study, the effective thermal conductivity of binary mixture $k_{r,\text{eff}}$ is corrected based on $k_{r,\text{eq}}$:

$$k_{r,\text{eff}} = X k_{r,\text{eq}} \tag{10}$$

where X is the correction factor of binary mixture and $k_{r,\text{eq}}$ is the effective radiation thermal conductivity of a single particle size bed.

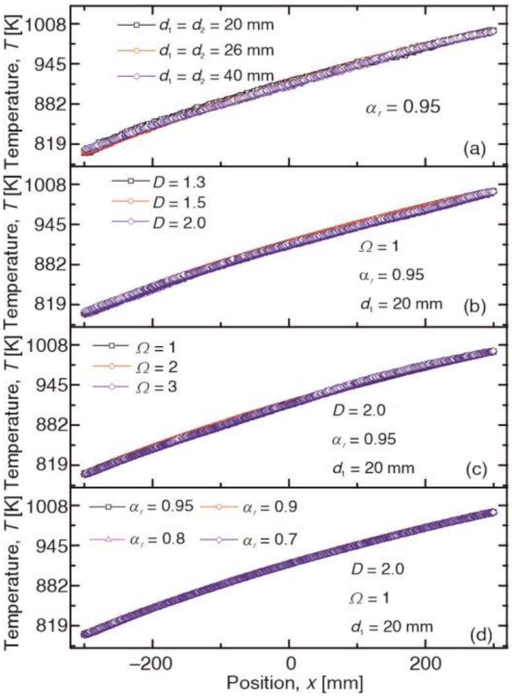

Figure 11. Temperature distribution in bed; (*a*) single size beds and (*b*)-(*d*) binary size particles beds

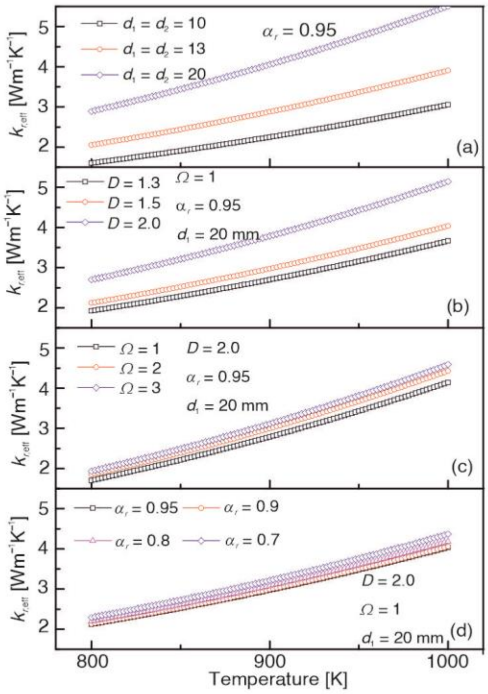

Figure 12. Effective thermal conductivity of bed; (*a*) single size granular beds and (*b*)-(*d*) binary size particles beds

According to the previous studies, $k_{r,\text{eq}}$ has a linear relationship with T^3 and particles diameter, as $k_{r,\text{eq}} = F_E \Lambda$, where $\Lambda = 4\sigma d_1 T^3$, F_E is the exchange factor. In our study, a simple relationship of F_E is assumed, $F_E = \zeta \varepsilon_r^k$, where, ζ and k are coefficients for absorptivity. Obviously, X is related to diameter ratio D and fraction ratio Ω. When $D = 1$ or $\Omega = 0$, $X = 1$, the binary mixture can degrade to single size granular bed. Based on this truth, we introduce the expression of X as following:

$$X = \frac{m + D\Omega^n}{m + \Omega^n} \tag{11}$$

where m and n are coefficients in correction factor of binary mixture.

Hence, the eq. (6) can be rewritten as:

$$k_{r,\text{eff}} = 4\zeta\sigma d_1 \varepsilon_r^k \frac{m + D\Omega^n}{m + \Omega^n} T^3 \tag{12}$$

Fitting is carried out based on the influence of ε_r, D, Ω, and T on $k_{r,\text{eff}}$, as shown in fig. 12, obtaining $\zeta = 2/3$, $m = 0.461$, $n = 1$, and $k = 0.27$. Therefore, $k_{r,\text{eff}}$ can be shown in eq. (9), which gives the correction formula of thermal conductivity in binary particle size bed:

$$k_{r,\text{eff}} = \frac{8}{3}\sigma d_1 \varepsilon_r^{0.27} \frac{0.461 + D\Omega}{0.461 + \Omega} T^3 \tag{13}$$

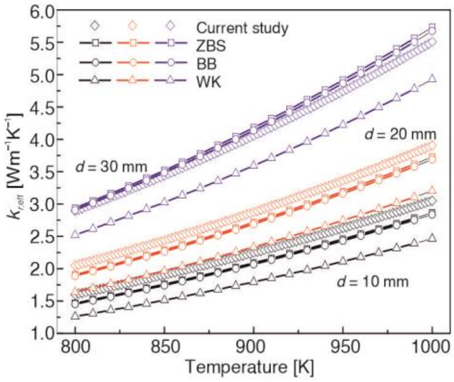

Figure 13. Comparison of the thermal conductivity between the current study and previous models

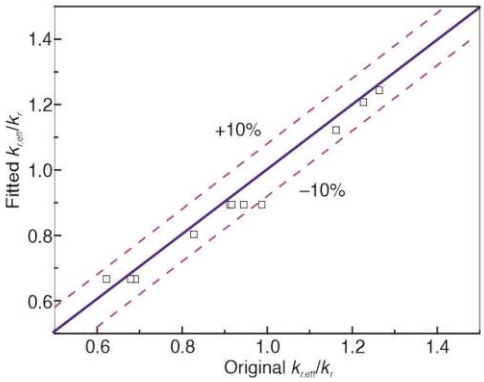

Figure 14. Accuracy of effective thermal conductivity fitting

Figure 14 shows the accuracy of the fitting formula, eq. (13). The fitting formula in this work is in good agreement with the original calculated results, and the fitting error is less than 10%. Furthermore, eq. (13) has extended the radiation thermal conductivity calculation to the binary-size mixture, which is more in line with the actual situation.

The results obtained in this paper provide a basis for the calculation of radiative heat transfer in the high temperature granular bed. It should be noted that the influence of the heat transfer of the granular material itself on the radiative heat transfer has not been considered in the paper. Therefore, the results obtained from this paper are suitable for the high-temperature granular beds dominated by radiation. When the thermal conductivity of particle material is small or the radiation heat is not dominant, namely, the effective thermal conductivity of radiation is at the same level as the thermal conductivity of the particle material [18], the influence of thermal conductivity on radiative heat transfer needs to be furtherly considered.

Conclusions

The effective view factor and effective thermal conductivity of high temperature binary-size granular bed were studied in this paper. The effective view factor decreases exponentially with the increase of the particle distance. As for a packed granular bed, the view factor is almost completely attenuated when particle interval is greater than their diameter. The surface characteristic of particle material also affects the radiative heat transfer, and the view factor decreases as the absorptivity of the granular material decreases. For a binary-size granular bed, the view factor of large particles increases with increasing particle size but is hardly affected by the solid fraction ratio of large to small particles. The empirical correlation formula for the view factors of randomly packed granular beds is given as eqs. (7) and (8) by fitting the MC calculation results.

The effective radiation thermal conductivity of the bed is proportional to the particle size d and third power of temperature T^3, and decreases with the increase in particle absorptivity. For a binary-size granular bed, the thermal conductivity increases with the increase in particle size ratio and volume ratio. Finally, the corrected formula for the calculation of effective radiation thermal conductivity of binary-size granular bed is given as eq. (13). Therefore, the paper may provide reference for the calculation of effective thermal conductivity involved in the heat transfer process of high temperature multicomponent particles.

Acknowledgment

The National Key Research and Development Program of China (2019YFC1905702), the National Natural Science Foundation of China (51972019) are duly acknowledged for their financial support.

References

[1] Antwerpen, W. V., *et al.*, A Review of Correlations to Model the Packing Structure and Effective Thermal Conductivity in Packed Beds of Mono-sized Spherical Particles, *Nuclear Engineering & Design*, *240* (2010), 7, pp. 1803-1818
[2] Zhang, Z., *et al.*, Design Aspects of the Chinese Modular High-Temperature Gas-Cooled Reactor HTR-PM, *Nuclear Engineering and Design*, 236 (2006), 5-6, pp. 485-490
[3] Liu, J., *et al.*, Thermal Energy Recovery from High-Temperature Blast Furnace Slag Particles, *International Communications in Heat and Mass Transfer, 1* (2015), 69, pp. 23-28
[4] Stenberg, V., *et al.*, Evaluation of Bed-to-Tube Surface Heat Transfer Coefficient for a Horizontal Tube in Bubbling Fluidized Bed at High Temperature, *Powder Technology, 352* (2019), June, pp. 488-500
[5] Pitso, M. L., Characterisation of Long Range Radiation Heat Transfer in Packed Pebble Beds, Ph. D. thesis, North-West University, Evanston, USA, 2011
[6] Felske, J. D., Approximate Radiation Shape Factors Between Two Spheres, *Journal of Heat Transfer*, *100* (1978), 3, pp. 547-548
[7] Howell, J. R., The Monte Carlo Method in Radiative Heat Transfer, *Journal of Heat Transfer*, *120* (1998), 3, pp. 547-560
[8] Wu, H., *et al.*, Numerical Simulation of Heat Transfer in Packed Pebble Beds: CFD-DEM Coupled with Particle Thermal Radiation, *Int. Journal of Heat and Mass Transfer*, *110* (2017), July, pp. 393-405
[9] Wu, H., *et al.*, Analysis and Evaluations of Four Models of Thermal Radiation for Densely Packed Granular Systems, *Chemical Engineering Science*, *211* (2020), 115309
[10] Chen, J. C., *et al.*, Radiant Heat Transfer in Packed Beds, *AIChE Journal*, *9* (1963), 1, pp. 35-41
[11] Argo, W. B., Smith J. M., Heat Transfer in Packed Beds, *Chemical Engineering Progress*, *49* (1953), 3, pp. 443-451
[12] Wakao, N., Kato, K., Effective Thermal Conductivity of Packed Beds, *Journal of Chemical Engineering of Japan*, *2* (1969), 1, pp. 24-33
[13] Kasparek, G., Vortmeyer, D., Wärmestrahlung in Schüttungen aus Kugeln Mit Vernachlässigbarem Wärmeleitwiderstand, *Wärme-und Stoffübertragung*, *9* (1976), 2, pp. 117-128
[14] Vortmeyer, D., Radiation in Packed Solids, *Proceedings,* 6th International Heat Transfer Conf., Toronto, Canada, 1978, Vol. 6, pp. 525-529
[15] Antwerpen, W. V., *et al.*, Multi-Sphere Unit Cell Model to Calculate the Effective Thermal Conductivity in Packed Pebble Beds of Mono-Sized Spheres, *Nuclear Engineering & Design*, *247* (2012), 6, pp. 183-201
[16] Johnson, E., *et al.*, A Monte Carlo Method to Solve for Radiative Effective Thermal Conductivity for Particle Beds of Various Solid Fractions and Emissivities, *Journal of Quantitative Spectroscopy and Radiative Transfer*, *250* (2020), 107014
[17] Zhou, J., *et al.*, A Boundary Element Method for Evaluation of the Effective Thermal Conductivity of Packed Beds, *Journal of Heat Transfer*, *129* (2007), 3, pp. 363-371
[18] Singh, B. P., Kaviany M., Effect of Solid Conductivity on Radiative Heat Transfer in Packed Beds, *International Journal of Heat & Mass Transfer*, *37* (1994), 16, pp. 1159-1168
[19] Chen, L., *et al.*, Effective Thermal Property Estimation of Unitary Pebble Beds Based on a CFD-DEM Coupled Method for A Fusion Blanket, *Plasma Science and Technology*, *17* (2015), 12, pp. 1083-1087
[20] Chen, L., *et al.*, Investigation of Effective Thermal Conductivity for Pebble Beds by One-way Coupled CFD-DEM Method for CFETR WCCB, *Fusion Engineering and Design*, *106* (2016), May, pp. 1-8

[21] Mandal, D., *et al.*, Void Fraction and Effective Thermal Conductivity of Binary Particulate Bed, *Fusion Engineering and Design*, *88* (2013), 4, pp. 216-225
[22] Lai, J. F., *et al.*. Bayesian Inference for Solving a Class of Heat Conduction Problems, *Thermal Scienc*e, *25* (2021), 3B, pp. 2135-2142
[23] Wang, T., *et al.*, A Local Average Method for Stochastic Thermal Analysis Under Heat Conduction Conditions, *Thermal Science*, *23* (2019), 2B, pp. 899-911
[24] Yan, Z. Z., *et al.*, A New Method For Solving a Class of Heat Conduction Equations, *Thermal scienc*e, *19* (2015), 4, pp. 1205-1210
[25] Colomer, G., *et al.*, Three-Dimensional Numerical Simulation of Convection and Radiation in A Differentially Heated Cavity Using the Discrete Ordinates Method, *International Journal of Heat and Mass Transfer, 47* (2004), 2, pp. 257-69
[26] Chai, J. C., *et al.*, Finite Volume Method for Radiation Heat Transfer, *Journal of Thermophysics & Heat Transfer*, 8 (1994), 3, pp. 419-425
[27] Fokou, A., *et al.*, Radiation Distribution in Inhomogeneous Atmosphere-Ocean System by Discrete Spherical Harmonics Method, *Journal of Quantitative Spectroscopy and Radiative Transfer, 270* (2021), 5, 107707
[28] Byun, D. Y., *et al.*, Thermal Radiation in A Discretely Heated Irregular Geometry Using the Monte-Carlo, Finite Volume, and Modified Discrete Ordinates Interpolation Method, *Numerical Heat Transfer: Part A: Applications, 37* (2000), 1, pp. 1-8
[29] Zehner, P., *et al.*, Einfluß der Wärmestrahlung und des Druckes auf den Wärmetransport in nicht durchströmten Schüttungen, *Chemie Ingenieur Technik, 44* (1972), 23, pp. 1303-1308
[30] Breitbach, G., Barthels, H., The Radiant Heat Transfer in the High Temperature Reactor Core after Failure of the Afterheat Removal Systems, *Nuclear Technology, 49* (1980), 3, pp. 392-399

Paper submitted: February 4, 2022
Paper revised: April 20, 2022
Paper accepted: April 28, 2022